Supplemental Material for Piezoelectric Electron-Phonon Interaction from *Ab Initio* Dynamical Quadrupoles: Impact on Charge Transport in Wurtzite GaN

Vatsal A. Jhalani,[1,*] Jin-Jian Zhou,[1,*] Jinsoo Park,[1] Cyrus E. Dreyer,[2,3] and Marco Bernardi[1,†]

[1] *Department of Applied Physics and Materials Science, Steele Laboratory, California Institute of Technology, Pasadena, California 91125, USA.*

[2] *Department of Physics and Astronomy, Stony Brook University, Stony Brook, New York 11794-3800*

[3] *Center for Computational Quantum Physics, Flatiron Institute, 162 Fifth Avenue, New York, New York 10010*

I. Calculation of dynamical quadrupoles in wurtzite GaN

As discussed in the main text, the dynamical quadrupoles are key to implementing the quadrupole e-ph interaction. The dynamical quadrupoles are denoted as $Q^{(\alpha\gamma)}_{\kappa\beta}$ in the main text (to simplify the notation), while here and in the following we use the notation $Q^{(2,\alpha\gamma)}_{\kappa\beta}$. We compute the dynamical quadrupoles through

$$Q^{(2,\alpha\gamma)}_{\kappa\beta} = i\Omega \left(\frac{\partial \overline{P}^{\mathbf{q}}_{\alpha,\kappa\beta}}{\partial q_\gamma}\bigg|_{\mathbf{q}=0} + \frac{\partial \overline{P}^{\mathbf{q}}_{\gamma,\kappa\beta}}{\partial q_\alpha}\bigg|_{\mathbf{q}=0} \right) , \tag{1}$$

which is Eq. (3) in the main text. The space group of wurtzite GaN is $P6_3mc$, with $2a$ and $2b$ Wyckoff positions occupied. Both sites have $3m$ point symmetry, and thus there are four independent nonzero elements in each atomic dynamical quadrupole tensor, as listed in Table SI. Thus we calculate

$$Q^{(2,22)}_{\kappa 2} = 2\Omega \overline{P}^{(1,2)}_{2,\kappa 2}\,, \quad Q^{(2,33)}_{\kappa 3} = 2\Omega \overline{P}^{(1,3)}_{3,\kappa 3}\,, \quad Q^{(2,11)}_{\kappa 3} = 2\Omega \overline{P}^{(1,1)}_{1,\kappa 3}\,, \quad Q^{(2,31)}_{\kappa 1} = \Omega \left[\overline{P}^{(1,1)}_{3,\kappa 1} + \overline{P}^{(1,3)}_{1,\kappa 1} \right].$$

The dynamical quadrupole calculations were conducted on the 4-atom primitive cell of GaN (see Fig. S1), using relaxed lattice parameters ($a = 3.187$ Å, $c = 5.192$ Å, and $u = 0.377\ c/a$). The methodology of Ref. 1 was implemented in the ABINIT code. The q_i derivatives were obtained using finite differences by computing $\overline{P}^{\mathbf{q}}_{\alpha,\kappa\beta}$ at $q_i = 0$, 0.01, and 0.02 (in units of $2\pi/a_i$). The quadrupole calculations employed scalar relativistic norm-conserving pseudopotentials [2, 3] generated by Pseudo Dojo [4]. All efforts were made to maintain consistency between the dynamical quadrupole calculations in ABINIT and the Quantum ESPRESSO (QE) DFT/DFPT calculations discussed in the main text. In particular, identical structures, the same exchange-correlation functional (PBEsol), and the same type of pseudopotential (ONCVPSP) generated using identical parameters were used. At the time of writing, no implementation for calculating dynamical quadrupoles that includes spin-orbit coupling (SOC) exists. We explicitly verified that the difference between the Born effective charges computed with and without SOC is negligible in GaN, and we find that the e-ph coupling strengths computed with dynamical quadrupoles match closely with DFPT calculations with SOC (see Fig. 1), suggesting that the effect of SOC on the dynamical quadrupoles is negligible in GaN. We used a Monkhorst-Pack [5] **k**-point grid of $10 \times 10 \times 8$ for the Brillouin zone sampling and a plane-wave kinetic energy cutoff of 80 Ha. The results of the dynamical quadrupole calculations are given in Table SII.

TABLE SI. Components of the quadrupole tensor for $3m$ site symmetry.

β \ $\alpha\gamma$	**11**	**22**	**33**	**23**	**13**	**12**
1	0	0	0	0	0	$Q^{(2,12)}_{\kappa 1} = -Q^{(2,22)}_{\kappa 2}$
2	$Q^{(2,11)}_{\kappa 2} = -Q^{(2,22)}_{\kappa 2}$	$Q^{(2,22)}_{\kappa 2}$	0	$Q^{(2,32)}_{\kappa 2} = Q^{(2,31)}_{\kappa 1}$	0	0
3	$Q^{(2,11)}_{\kappa 3}$	$Q^{(2,22)}_{\kappa 3} = Q^{(2,11)}_{\kappa 3}$	$Q^{(2,33)}_{\kappa 3}$	0	0	0

* V.J. and J.-J.Z. contributed equally to this work

† Corresponding author: bmarco@caltech.edu

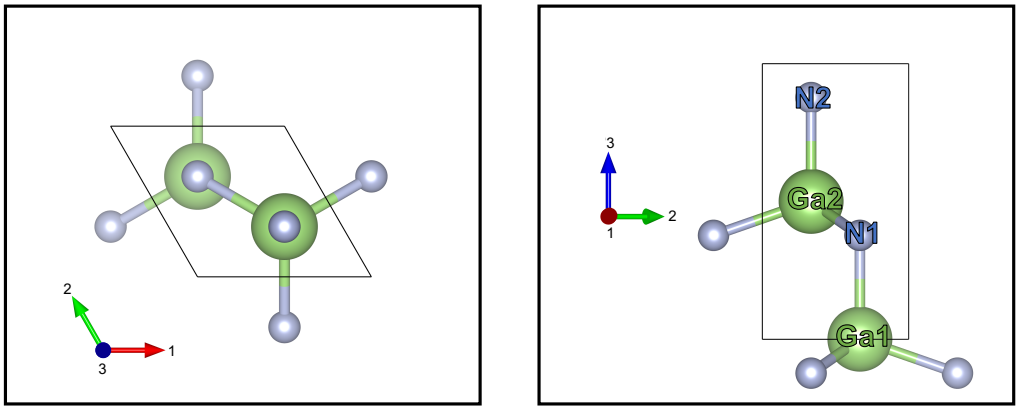

FIG. S1. Wurtzite GaN primitive cell structure used to compute the dynamical quadrupoles.

TABLE SII. Dynamical quadrupoles (e Bohr units) for the primitive cell of wurtzite GaN.

	$\kappa = \text{Ga1}$	$\kappa = \text{Ga2}$	$\kappa = \text{N1}$	$\kappa = \text{N2}$
$Q^{(2,22)}_{\kappa 2}$	4.120	−4.120	−1.168	1.168
$Q^{(2,33)}_{\kappa 3}$	5.360	5.360	−0.389	−0.389
$Q^{(2,11)}_{\kappa 3}$	−2.369	−2.369	−0.338	−0.338
$Q^{(2,31)}_{\kappa 1}$	−2.539	−2.539	−0.047	−0.047

It has been demonstrated [6–8] that the clamped-ion piezoelectric coefficients $e_{\alpha\beta\gamma}$ can be written as sublattice sums of the dynamical quadrupoles

$$e_{\alpha\beta\gamma} = -\frac{1}{2\Omega}\sum_{\kappa}\left[Q^{(2,\alpha\gamma)}_{\kappa\beta} - Q^{(2,\gamma\beta)}_{\kappa\alpha} + Q^{(2,\beta\alpha)}_{\kappa\gamma}\right]. \tag{2}$$

In the ABINIT code [9], the piezoelectric response can be calculated via DFPT, where a strain perturbation is applied using the metric formalism of Hamann *et al.* [10]. We use this implementation, and employ Eq. (2) as an independent test of our calculations of the dynamical quadrupoles. Specifically, we should find that for wurtzite GaN (point group $6mm$)

$$e_{333} = -\sum_{\kappa}\overline{P}^{(1,3)}_{3,\kappa 3}, \quad e_{311} = -\sum_{\kappa}\overline{P}^{(1,1)}_{3,\kappa 1}, \quad e_{113} = -\sum_{\kappa}\overline{P}^{(1,3)}_{1,\kappa 1}, \quad e_{222} = 0 = -\sum_{\kappa}\overline{P}^{(1,2)}_{2,\kappa 2}.$$

We see from Table SIII that the two methods of calculating the piezoelectric coefficients agree very closely, confirming the accuracy of the dynamical quadrupoles employed in this work.

We also compute the clamped-ion piezoelectric coefficients using the QE strain perturbation approach, with the same computational settings as in ABINIT. The computed values from QE are in excellent agreement with those from ABINIT. For example, the e_{333} coefficient from our QE strain perturbation calculations is -0.92276 C/m^2, almost identical to the ABINIT strain result (-0.9228 C/m^2) and in very close agreement (within 0.03%) to the ABINIT quadrupole value of -0.9231 C/m^2, as shown in Table SIII. These results clearly demonstrate the consistency between our QE and ABINIT calculations. We additionally compared e_{333} computed with and without SOC using QE, obtaining values of -0.92276 C/m^2 without SOC and -0.92281 C/m^2 with SOC, which show that SOC has a negligible effect on the piezoelectric coefficients and thus on the dynamical quadrupoles. Therefore, although the quadrupoles are computed without SOC in ABINIT, they can be safely applied to calculations with SOC in QE given the negligible role of SOC and the consistency of our ABINIT and QE calculations.

TABLE SIII. Piezoelectric coefficients (units of C/m^2) for the primitive cell of wurtzite GaN, calculated using the ABINIT strain perturbation and compared with the quadrupole summation method.

	e_{333}	e_{113}	e_{311}	e_{222}
strain	−0.9228	0.5041	0.4562	0.0000
quadrupole	−0.9231	0.5027	0.4579	0.0000

II. Computational details for *ab initio* e-ph relaxation times and mobilities in wurtzite GaN

We carefully converge the e-ph scattering rates $\Gamma_{n\mathbf{k}}$ using the PERTURBO code [11]. We compute $\Gamma_{n\mathbf{k}}(T)$ from the lowest order e-ph self-energy on a $200 \times 200 \times 200$ **k**-point Monkhorst-Pack [5] grid for electrons and a $100 \times 100 \times 100$ **k**-point grid for holes, using an 8 meV Gaussian broadening to approximate the δ functions. In all calculations the Fermi energy at each temperature was set to ensure a 1×10^{17} cm^{-3} carrier concentration for both electrons and holes. Varying the concentration below this value does not affect the mobility results, which can be regarded as an intrinsic mobility limit in GaN. For each **k**-point, the long-range contribution to the scattering rate was converged with 2×10^6 Cauchy-distributed **q**-points [12]. The remaining scattering rate contribution was converged with 1×10^5 and 2×10^5 uniformly distributed **q**-points for electrons and holes, respectively. The RTA mobilities were obtained using the relaxation times $\tau_{n\mathbf{k}}(T) = \Gamma^{-1}_{n\mathbf{k}}(T)$. The BTE was also solved iteratively [11], with a relative error threshold between consecutive iterations of 0.2% on a $200 \times 200 \times 200$ **k**-point grid for electrons and $80 \times 80 \times 80$ **k**-point grid for holes. The grids were converged to within $< 0.5\%$ error on the mobilities.

III. Comparison with Macroscopic Piezoelectric Coupling

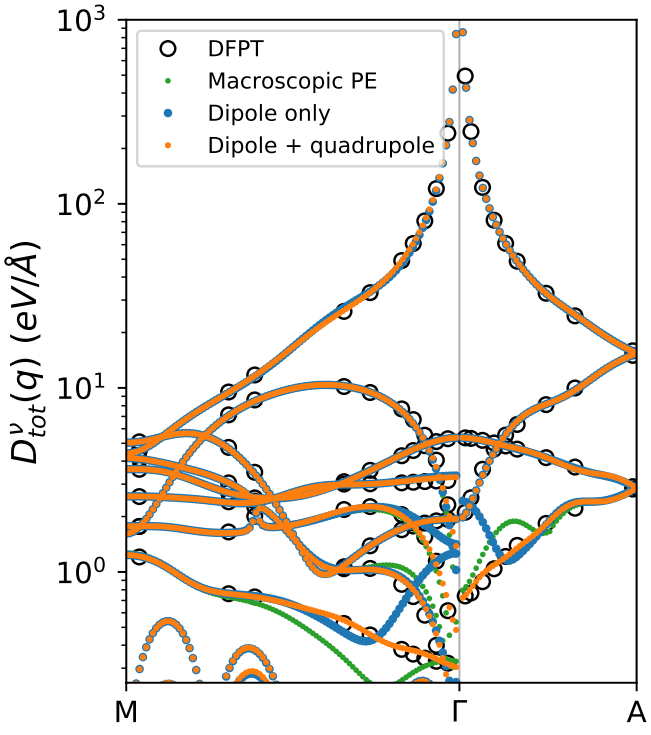

FIG. S2. Mode-resolved $D^{\nu}_{\mathrm{tot}}(\mathbf{q})$ along high-symmetry lines. We show e-ph matrix elements computed from DFPT as a benchmark (black circles), and obtained from Wannier interpolation plus the generalized Fröhlich interaction (blue), Wannier interpolation with the Fröhlich plus quadrupole interactions (orange), and Wannier interpolation plus the macroscopic PE coupling (green) given in Eq. (6) of the main text.

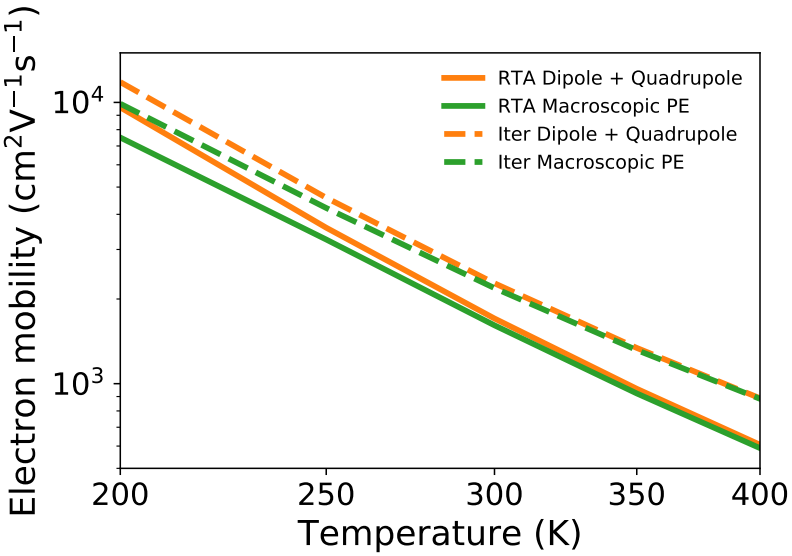

FIG. S3. Electron mobilities in wurtzite GaN, computed in the [1000] plane. Shown are computed results obtained with the RTA (solid lines) and iterative BTE (dashed lines), both with dipole plus quadrupole interactions (orange) and the macroscopic PE coupling (green) given in Eq. (6) of the main text.

[1] C. E. Dreyer, M. Stengel, and D. Vanderbilt, Phys. Rev. B **98**, 075153 (2018).
[2] D. R. Hamann, Phys. Rev. B **88**, 085117 (2013).
[3] J. P. Perdew, A. Ruzsinszky, G. I. Csonka, O. A. Vydrov, G. E. Scuseria, L. A. Constantin, X. Zhou, and K. Burke, Phys. Rev. Lett. **100**, 136406 (2008).
[4] M. van Setten, M. Giantomassi, E. Bousquet, M. Verstraete, D. Hamann, X. Gonze, and G.-M. Rignanese, Comput. Phys. Commun. **226**, 39 (2018).
[5] H. J. Monkhorst and J. D. Pack, Phys. Rev. B **13**, 5188 (1976).
[6] M. Stengel, Phys. Rev. B **88**, 174106 (2013).
[7] R. M. Martin, Phys. Rev. B **5**, 1607 (1972).
[8] M. Royo and M. Stengel, Phys. Rev. X **9**, 021050 (2019).
[9] X. Gonze, F. Jollet, F. Abreu Araujo, D. Adams, B. Amadon, T. Applencourt, C. Audouze, J.-M. Beuken, J. Bieder, A. Bokhanchuk, E. Bousquet, F. Bruneval, D. Caliste, M. Côté, F. Dahm, F. Da Pieve, M. Delaveau, M. Di Gennaro, B. Dorado, C. Espejo, G. Geneste, L. Genovese, A. Gerossier, M. Giantomassi, Y. Gillet, D. Hamann, L. He, G. Jomard, J. Laflamme Janssen, S. Le Roux, A. Levitt, A. Lherbier, F. Liu, I. Lukačević, A. Martin, C. Martins, M. Oliveira, S. Poncé, Y. Pouillon, T. Rangel, G.-M. Rignanese, A. Romero, B. Rousseau, O. Rubel, A. Shukri, M. Stankovski, M. Torrent, M. Van Setten, B. Van Troeye, M. Verstraete, D. Waroquiers, J. Wiktor, B. Xu, A. Zhou, and J. Zwanziger, Comput. Phys. Commun. **205**, 106 (2016).
[10] D. R. Hamann, X. Wu, K. M. Rabe, and D. Vanderbilt, Phys. Rev. B **71**, 035117 (2005).
[11] J.-J. Zhou, J. Park, I.-T. Lu, I. Maliyov, X. Tong, and M. Bernardi, "Perturbo: a software package for ab initio electron-phonon interactions, charge transport and ultrafast dynamics," arXiv:2002.02045.
[12] J.-J. Zhou and M. Bernardi, Phys. Rev. B **94**, 201201(R) (2016).